

Climatological features of WRF-simulated tropical cyclones over the western North Pacific

Dasol Kim · Chun-Sil Jin · Chang-Hoi Ho ·
Jinwon Kim · Joo-Hong Kim

Received: 11 February 2014 / Accepted: 11 November 2014 / Published online: 21 November 2014
© Springer-Verlag Berlin Heidelberg 2014

Abstract Tropical cyclones (TCs) over the western North Pacific (WNP) are simulated for the 29 TC seasons of July–October from 1982 to 2010 using the regional Weather Research and Forecasting (WRF) model nested within global WRF model simulations. Averaged over the entire 29-year period, the nested global–regional WRF has reasonably simulated the climatology of key TC features such as the location/frequency of genesis and tracks. The dynamical and thermal structures of the simulated TCs are weaker than observations owing to the coarse spatial resolution of the regional WRF (50 km × 50 km). TC frequencies are somewhat underestimated over the East China Sea but are substantially overestimated over the South China Sea and the Philippine Sea with neighboring oceans between 10°N and 15°N. Categorization of the simulated TCs into six clusters based on the observed TC clusters and the associated large-scale circulation show that the nested simulation depicts the observed TC characteristics well except for two clusters associated with TCs traveling from the Philippine Sea to the East China Sea. Errors in the simulated TC genesis and tracks are mostly related to these two clusters. In the simulation, the monsoon confluent zone over the Philippine Sea is too strong, and the mid-latitude jet stream expands farther south than that in the

observations. Overall results from this study suggest that the nested global–regional WRF can be useful for studying the TC climatology over the WNP.

Keywords Weather Research and Forecasting (WRF) model · Tropical cyclone · Western North Pacific · Fuzzy clustering

1 Introduction

Tropical cyclones (TCs) are among the most destructive natural disasters and cause substantial losses in both human lives and the economy. The western North Pacific (WNP) region experiences the most vigorous TC activities with frequent landfalls along the East Asian coast (Kim et al. 2005a, b; Park et al. 2014). It is critical to improve the accuracy of TC forecasts as well as to understand the processes involved in the lifespan of TCs over the WNP for mitigating damages from TC-induced natural disasters. A number of previous studies have examined the climatology of TC activity over the target region and various climate changes closely linked to TC activities (e.g. Gray 1977; Chan 2000; Wang and Chan 2002; Ho et al. 2004, 2009; Camargo and Sobel 2005; Kim et al. 2008).

The simulation of TCs by using numerical models has been a great challenge. TC-like vortices have been previously simulated in atmospheric general circulation models (AGCMs; Walsh et al. 2010). Nevertheless, AGCMs generally underestimate TC intensities and poorly simulate key TC activities such as genesis locations and tracks mainly due to their coarse spatial resolutions. With recent advancements in numerical modeling techniques, there have been significant achievements in TC-related studies that use dynamical models. For example, Manganello et al. (2012)

D. Kim · C.-S. Jin · C.-H. Ho (✉)
Climate Physics Laboratory, School of Earth and Environmental
Sciences, Seoul National University, Seoul 151-747, South Korea
e-mail: hoch@cpl.snu.ac.kr

J. Kim
Department of Atmospheric and Oceanic Sciences, UCLA,
Los Angeles, CA, USA

J.-H. Kim
Korea Polar Research Institute, Incheon, South Korea

showed that a 10-km resolution AGCM can simulate TC intensity and structure with reasonable accuracy. Despite such success in simulating TCs, fine-resolution AGCMs are too costly for most research groups with limited computational resources.

An alternative to fine-resolution AGCM simulations may be the use of regional models nested within coarse-resolution, large-scale analyses or AGCM data. Such one-way nested regional modeling has been improved significantly in recent years and is widely used in operational weather predictions and regional climate research. Results from regional climate models (RCMs) nested within AGCMs are useful for studying regional-scale disturbances under specific large-scale circulations, which represent TC analysis well (e.g. Camargo et al. 2007a; Stowasser et al. 2007; Au-Yeung and Chan 2011; Jin et al. 2013). The genesis and movements of TCs, as well as the key processes associated with TC activities, strongly depend on regional environments. The ability of a model to simulate TC genesis and track generally vary for different basins. Manganello et al. (2012) showed that TC simulations are better in the North Atlantic than in the WNP and that the model errors are smaller for the North Atlantic but larger for the WNP when the resolution of AGCM is very fine (up to 10 km). Thus, RCMs may be optimized for a region by tuning physics parameterizations to fit the large-scale environments specific to the region; this is not generally possible for AGCMs.

The present study examines the simulated TC activity for the WNP region by using a combination of global and regional Weather Research and Forecasting (WRF) models. WRF has been widely used in short-term TC forecasting (e.g. Davis et al. 2008; Fierro et al. 2009; Gentry and Lackmann 2010; Cha et al. 2011; Potty et al. 2012) or regional climate studies (e.g. Waliser et al. 2011; Mearns et al. 2012; Kim et al. 2013), but its use on TC climatology has been limited to a small number of studies (Jin et al. 2013, JH13 hereafter). The global–regional WRF experiment is an extension of previous WRF model studies. The global WRF model which is used as boundary conditions for regional domain can simulate reasonably climatological features of large-scale environment, such as zonal wind, temperature, precipitation distribution (Shin et al. 2010). Recent studies on tropical channel model (Skok et al. 2010; Ray et al. 2011; Tulich et al. 2011) which is similar to global WRF in that they do not require eastern and western lateral boundary condition also show similar simulation results for large-scale environments compared to the global–regional WRF. Therefore, the examination of ability to simulate TC climatology using global and regional WRF model is useful in regional climate research for East Asian and WNP regions.

Previous studies on simulating TC activities using GCMs and RCMs generally focused on the mean

characteristics of all simulated TCs, typically as a part of model/parameterization evaluations. The mean properties of the simulated TCs, however, are insufficient for measuring the performance of a model, because key TC properties such as the frequency and location of genesis, tracks, intensities, and lifespans vary widely among TCs. TCs can be categorized into specific types according to their properties (Camargo et al. 2007b, c; Nakamura et al. 2009; Kim et al. 2011). Such TC types can represent individual TCs more effectively so that more specific information can be obtained when TC activity is investigated according to the TC types in simulations. This study uses the fuzzy *c*-means clustering method (Kim et al. 2011) to categorize the simulated TCs by their track patterns. The climatology of TC activities and WRF limitations in simulating important TC characteristics are investigated by comparing the simulated TC clusters with observations. The rest of this paper is organized as follows. Section 2 describes the data and fuzzy clustering used in this study; Sect. 3 provides the TC structures, total TC activities, and the characteristics of TC clusters simulated by using WRF; and the summary and discussions are presented in Sect. 4.

2 Data and methodology

2.1 Data

The TC best-track data recorded from the Regional Specialized Meteorological Centers (RSMC) Tokyo–Typhoon Center cover the period from 1951 to the present for the WNP region and are used for assessment of TC activity simulation during the TC seasons (July through October) of 1982–2010. The three grades of TCs—tropical depressions, tropical storms, and typhoons—with durations greater than 48 h were considered for the present analyses. The National Centers for Environmental Prediction (NCEP) reanalysis-2 data (Kanamitsu et al. 2002) are used for initial boundary condition of global WRF and diagnostic analysis for the period 1982–2010. The variables used for diagnostic analyses of the large-scale environment (in Sect. 3.3) include zonal and meridional winds at the 200- and 850-hPa levels, geopotential heights at 500 hPa, and relative humidity at 600 hPa. These atmospheric variables are widely used for evaluating TC simulations and are closely related with TC activities (Camargo et al. 2007a; Stowasser et al. 2007; Au-Yeung and Chan 2011). Optimal Interpolation Sea Surface Temperature (OISST) data from the National Oceanic Atmospheric Administration (NOAA) (Reynolds et al. 2002; <http://www.esrl.noaa.gov/psd/data/gridded/data.noaa.oisst.v2.html>) are used to provide the lower boundary condition to the simulation.

2.2 Model simulation and TC detection

The model simulation is identical to the control experiment we reported in a previous study (JH13). The global and regional WRF model version 3.3 (Skamarock et al. 2008) was run for June 21–October 31 for the 29-year period of 1982–2010. There is a 10-day spin up period, June 21–June 30, and the simulation is analyzed from July to October in which about 70 % of the observed TCs over the WNP basin are generated. To simulate the TC activity over the WNP (0°–60°N and 100°E–180°), the global WRF simulation with a 150-km horizontal resolution was downscaled by using a one-way nested regional WRF model at a 50-km horizontal resolution, which is the same configuration depicted as Fig. 2 in JH13. Both the global and regional models were configured with 27 vertical layers with a domain-top pressure of 50 hPa. The NCEP reanalysis-2 data were used to obtain the initial condition, and the OISST data were prescribed at time step of 1 day. The physical parameterization schemes used are the same as those used in Cha et al. (2011): Kain–Fritsch convective parameterization scheme (Kain and Fritsch 1990), WRF single-moment 3-class microphysics (WSM3) scheme (Hong et al. 2004), NCAR Community Atmosphere Model (CAM 3.0) radiation scheme (Collins et al. 2004), Yonsei University (YSU) planetary boundary layer scheme (Hong et al. 2006), and Noah land surface model (Chen and Dudhia 2001).

The detection and tracking methods for TCs in the simulation were the same as those used in JH13 and included the following parameters: (1) the center of the TC is a local minimum of sea level pressure; (2) the maximum surface wind speed exceeds 17 m s^{-1} ; (3) the local maximum of 850-hPa relative vorticity exceeds $4.9 \times 10^{-5} \text{ s}^{-1}$; (4) the sum of the temperature deviations at 300, 500, and 700 hPa exceeds 1.7 K, which suggests a warm-core threshold; and (5) the maximum wind speed at 850 hPa is higher than that at 300 hPa. All of these criteria were satisfied for a period of longer than 2 days. These criteria are similar to those of Camargo et al. (2007a) and Oouchi et al. (2006), but the thresholds are adjusted so that the number of detected TCs in the simulation is closest to that in the observation.

2.3 TC pattern clustering

Key TC characteristics such as the genesis frequency and intensity, as well as similar large-scale environments, vary according to track patterns (Harr and Elsberry 1991; Hodanish and Gray 1993; Elsner and Liu 2003; Camargo et al. 2007b, c; Kim et al. 2011). Thus, clustering TCs according to their track patterns is reasonable for comparison with observations to measure model performance. This study used fuzzy clustering to classify the observed

and simulated TCs according to track patterns. Kim et al. (2011) showed that fuzzy clustering can categorize TC track patterns of vague cluster boundaries. The same algorithm as that reported by Bezdek (1981) and Kim et al. (2011) was used in this study.

In fuzzy clustering, the membership coefficients indicating how close the location of the data member is to the cluster center vary from 0 to 1. The cluster centers are defined as the mean of all TC tracks weighted by the membership coefficient. A higher membership coefficient implies a stronger belongingness of the TC track with the cluster. The optimum number of clusters is determined by using the following four scalar validity indices applied in Kim et al. (2011): partition coefficient (Bezdek 1981), partition index (Bensaid et al. 1996), separation index (Xie and Beni 1991), and Dunn index (1973). For direct comparisons of the simulated clusters against observations, the cluster centers obtained from the observed TCs were used as the cluster centers in classification of the simulated TCs. That is, a simulated TC track was assigned to the observed TC cluster of which the simulated TC track showed the largest membership coefficient (i.e., largest similarity). In addition, the classification of simulated TCs using cluster centers obtained from the simulated TCs was also conducted. The latter method applied to simulated TCs showed similar results from the former method (not shown), but only the results from the former method is analyzed for the purpose of comparison using the same standards (i.e., observed TC cluster).

3 Results

3.1 Structure and intensity of TC in WRF

Prior to investigating the climatology of TC activities over the WNP, we examined how the model simulates the structure and intensity of TCs. Figure 1 shows the mean features of the five most intense TCs among the total 549 simulated TCs. The fields presented in Fig. 1 include (a) the horizontal distribution of tangential winds at 850 hPa, (b, c) the vertical distributions of azimuthally-averaged tangential and radial winds, and (d) the vertical temperature anomaly (deviation from the mean temperature over a 10° radius). The composite of the five most intense TCs was obtained by following a method analogous to that used in Bengtsson et al. (2007) and Manganello et al. (2012). The 850-hPa tangential winds suggest strong cyclonic circulation (positive sign indicates cyclonic flow) and significant asymmetry in the west–east direction (Fig. 1a). The tangential wind speed reaches a maximum value of 60 m s^{-1} to the east of TC center, whereas it is weaker to the west of the TC center. These results are well known TC observations (Frank 1977;

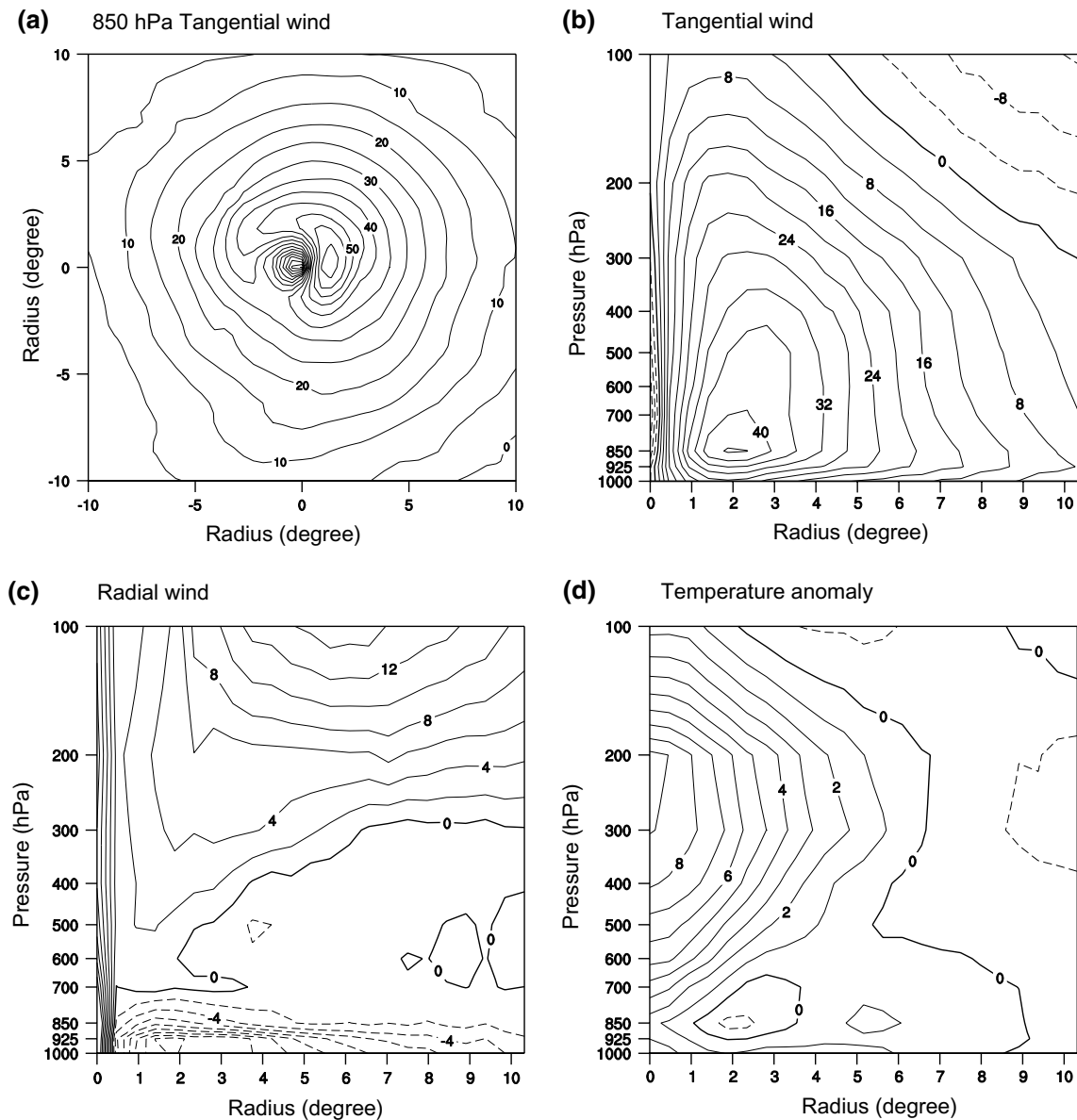


Fig. 1 Horizontal and vertical structure of **a** tangential wind at 850-hPa level, azimuthally averaged, **b** tangential wind and **c** radial wind, and **d** temperature anomaly for the composite of the five most intense

TCs. The units for wind speed and temperature are m s^{-1} and K, respectively. Negative values are *dashed*

Kept [2006a, b](#)). These cyclonic flows appeared clearly at all levels (Fig. 1b); the cyclonic flow was strongest at 850 hPa, and weakened with height within the troposphere. In the radial direction with respect to the center of the TC, the cyclonic flow was strongest at a distance of 2° and weakened as the radial distance increased. Anti-cyclonic flows were observed in the boundary regions of the upper troposphere. The vertical cross-section of the azimuthally averaged radial winds (Fig. 1c) indicated strong convergence in the lower troposphere (1,000–850 hPa) and divergence in the upper troposphere (400–100 hPa). The peak radial winds in the lower and upper troposphere are

-16.6 (i.e., towards the TC center) and 15.2 m s^{-1} (i.e., away from the TC center), respectively, and appear at a distance of 1.5° and 6° , respectively. Thus, the magnitude of the divergence in the upper troposphere is weaker than that of the convergence in the lower troposphere (magnitude of the radial-wind gradient, approximated from the peak wind speed and its location from the TC center, in the upper troposphere is smaller than that in the lower troposphere). The strong convergence near the surface and moderate divergence aloft can cause strong surface moisture fluxes at the surface and updrafts in the inner core. The warm core was located between 300 and 200 hPa with a maximum of 9 K

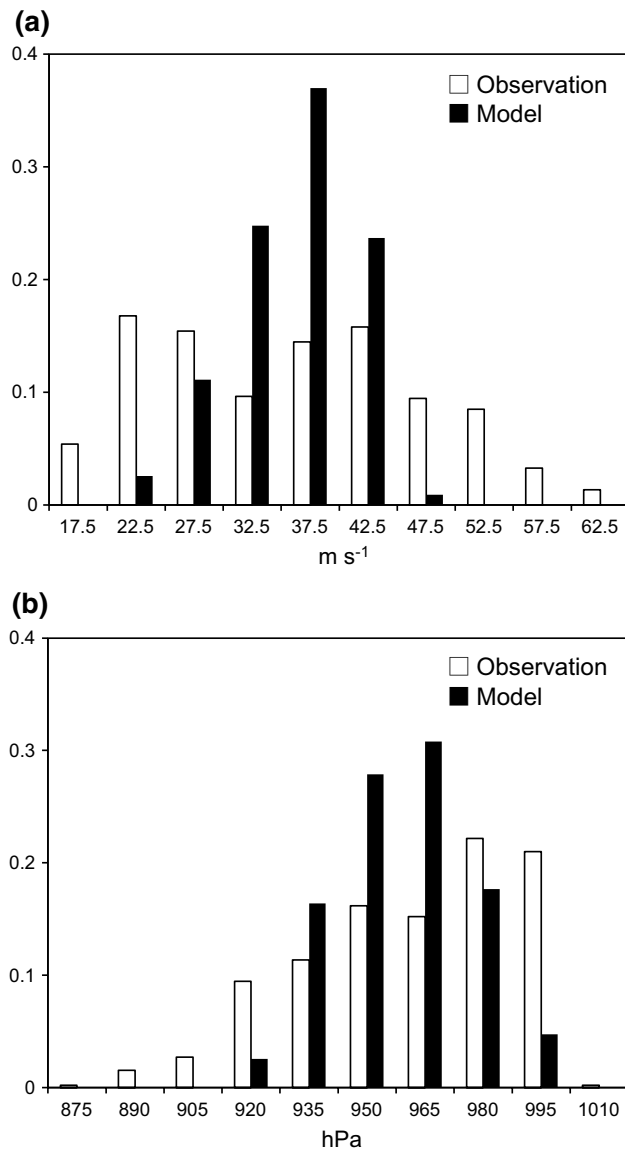


Fig. 2 Distribution of **a** maximum surface wind speed and **b** minimum sea level pressure for the simulation (*black bar*) and observation (*white bar*) during July–October of 1982–2010

(Fig. 1d), which is comparable to observation. These features were present, at least qualitatively, in all detected TCs of lesser strength.

Simulated TC intensity was examined to confirm whether the model can produce reliable TC strength despite the coarse horizontal resolution. The maximum surface wind speed and minimum central sea level pressure (SLP) during the lifetime of a TC can generally represent TC intensities (Wang and Wu 2004). Thus, the occurrence frequency of these two variables for the entire analysis period was assumed to indicate TC intensity. Figure 2 shows the frequency distribution of the maximum surface wind speed and the minimum central SLP in both simulations and

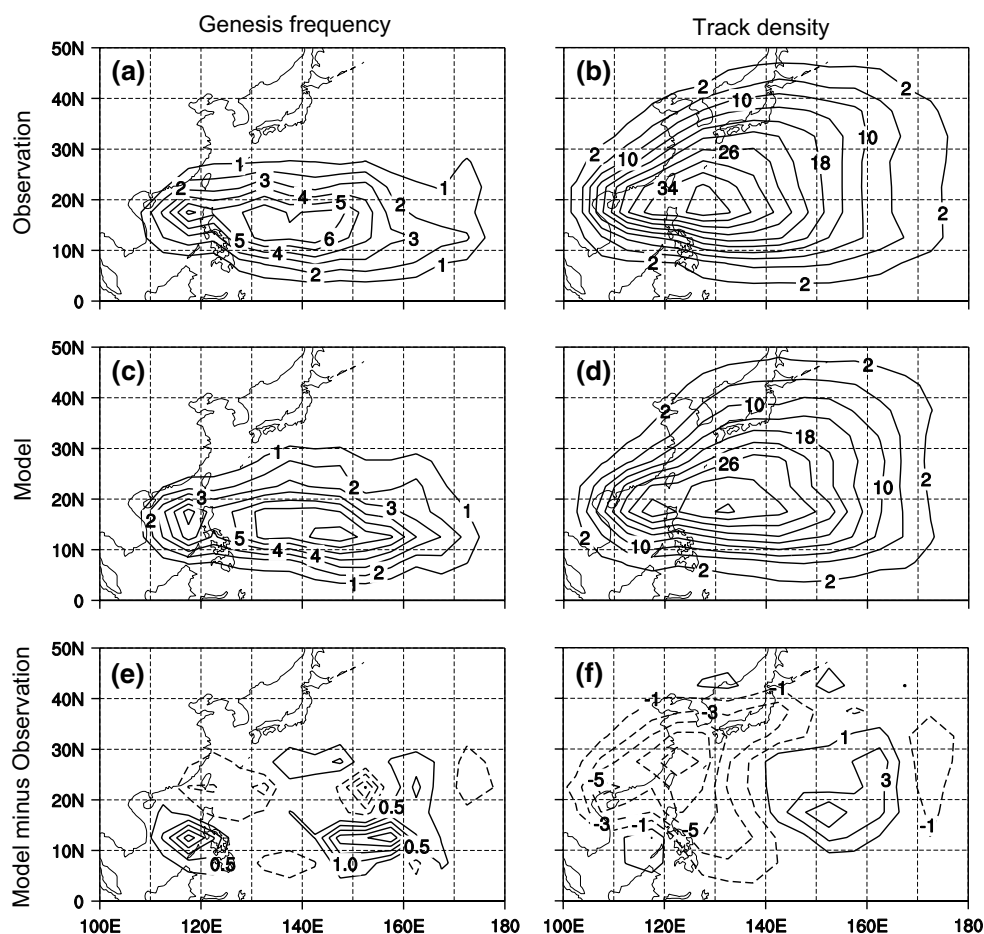
observations. The distribution of the observed maximum surface wind speed is characterized by a large variance with a bimodal shape with peaks at 22.5 and 42.5 m s^{-1} (Fig. 2a); the simulated distribution was significantly narrower (i.e., smaller variance) with a single peak at 37.5 m s^{-1} . The mean values of the maximum surface wind speed in the simulations (36.0 m s^{-1}) and the observations (34.7 m s^{-1}) were similar despite variations in their frequency distributions.

The variations in the frequency distribution of the minimum central SLP between observation and simulation were similar to those for the maximum wind speed (Fig. 2b). The observed distribution peaked at 980 hPa with large variance; however, the simulated distribution peaked at 965 hPa with much smaller variance (i.e., stronger intensity and narrower distribution). Similarly as the peak wind speed, the simulated mean central SLP minimum (959.1 hPa) agrees well with the observed value (961.6 hPa), although the frequencies for both weak (≥ 980 hPa) and strong (≤ 920 hPa) TCs are underestimated. Thus, the present model run with a 50-km horizontal resolution was limited in generating strong TCs with maximum surface winds of 47.5 m s^{-1} or a minimum central SLP of 920 hPa. Horizontal resolutions finer than 10 km may be needed to simulate extremely strong TCs comparable to observations (Davis et al. 2008; Fierro et al. 2009; Manganello et al. 2012). The relatively smaller frequency of weak TCs in the simulation also implies that simulated TCs are easily intensified upon generation. The over-intensification of a TC in the simulation may have been due to the large-scale environments that are favorable to TC intensification, which will be discussed in Sect. 3.3. The absence of ocean feedback in the model may have also contributed to the excessive strengthening of TCs because SST cooling by wind-induced upwelling that can suppress TC intensity was absent in the simulation (Bender et al. 1993; Bender and Ginis 2000).

3.2 Climatology of the simulated TC activities

To assess the capability of WRF in simulating TC activities, the climatology of those simulations was compared with observations. Figure 3 shows the frequency of TC genesis and track in observation (Fig. 3a, b), simulation (Fig. 3c, d), and their differences (Fig. 3e, f) for the TC seasons of 1982–2010. The genesis (track) frequency is defined as the average number of TCs per decade formed (traveled) in a $5^\circ \times 5^\circ$ grid box (e.g. Ho et al. 2004). The simulation effectively reproduced the observed local maxima in the genesis frequency in the South China Sea and Philippine Sea (Fig. 3a vs. c). The simulation, however, overestimated TC genesis over the southern South China Sea and southeastern Philippine Sea (8°N – 15°N and 145°E – 160°E) (Fig. 3e). At middle latitudes (north of 20°N), positive and

Fig. 3 Climatological mean of TC genesis (*left*) and track (*right*) frequencies over the WNP during July–October of 1982–2010 as number per decade in a $5^\circ \times 5^\circ$ grid box for **a**, **b** observation, **c**, **d** simulation, and **e**, **f** differences between simulation and observation



negative anomalies appeared concurrently. The track frequency pattern in the simulation was also similar to that in the observation (Fig. 3b vs. d) with local maxima near the western Philippine Sea (15°N – 25°N and 120°E – 140°E). The model underestimated the track frequency near coastal seas (west of 140°E), which resulted in a smaller number of TC landfalls than in observations, while the opposite is true for the open sea (east of 140°E) (Fig. 3f).

The large-scale circulation pattern examined in JH13 can explain these regional biases in TC activity. The control experiment in JH13, which is an identical model simulation as that in this study, showed that the monsoon trough was stronger in the simulation than that in the observation (Fig. 3e, f in JH13). This excessively strong monsoon trough in the WRF simulation reported in previous studies (Suzuki-Parker 2011; Tulich et al. 2011) appears to be related to the overestimation of TC genesis over the southern South China Sea and southeastern Philippine Sea. In addition, the western boundary of the simulated subtropical high stretched too far to the east compared with the observation. As the steering flow primarily modulates TC tracks, these errors were related to the underestimation (overestimation) of track frequency over coastal sea (open sea) in

the simulation. This interpretation, however, can provide only a superficial understanding of simulated TC activities. For more detailed analyses of the model errors, fuzzy clustering is employed to categorize the observed and simulated TCs in terms of track patterns. Comparison of the simulated and observed TC clusters are useful for understanding the causes of the errors because TC clusters possess distinct characteristics and mechanisms for their genesis (Kim et al. 2011).

Figure 4 shows the TC clusters derived from the observation and simulation. In this study, the observed 519 TCs are clustered into six clusters (left column of Fig. 4), unlike in the previous study (Kim et al. 2011) that classified the observed 855 TCs into seven clusters by using the same method. This different number of cluster is due to the different analysis periods (June–October of 1965–2010 in Kim et al. 2011 vs. July–October of 1982–2010 in this study). The analysis periods of the previous study cover those of the present study, which implies the TC samples in the present study are insufficient to be classified as seven clusters. Consequently the optimum number of cluster in this study is objectively determined as six according to the four scalar validity indices (Sect. 2.3). It should be noted

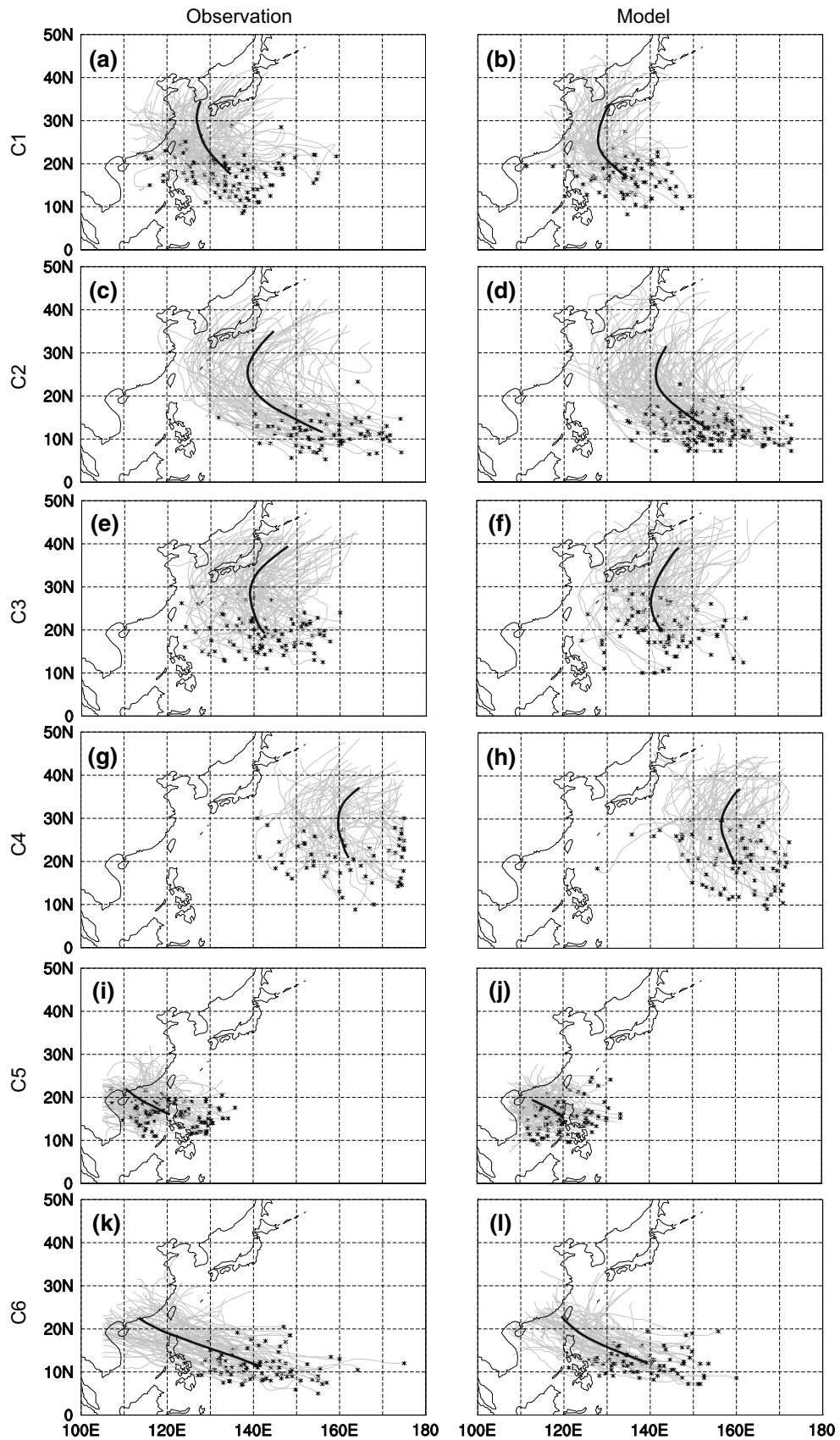


Fig. 4 Six TC clusters in the observation (*left*) and simulation (*right*) during July–October of 1982–2010. The *thick black lines* represent the mean TC tracks, and the *gray lines* represent the complete TC tracks for each cluster. The *marks* represent the genesis locations of TCs

Table 1 Statistics of characteristics of each TC cluster

	Maximum wind speed (m s^{-1})	Minimum central pressure (hPa)	Genesis frequency (per year)
C1	36.6 (+0.7)	956.9 (−3.2)	2.5 (−1.0*)
C2	38.3 (−4.9*)	952.0 (+11.7*)	4.6 (+1.8*)
C3	34.3 (+1.2)	960.3 (−6.5)	2.7 (−0.3)
C4	33.4 (+2.5)	964.3 (−8.9)	2.6 (+0.5)
C5	34.6 (+7.7*)	966.6 (−14.0*)	3.9 (+0.3)
C6	38.3 (−0.7)	956.5 (+3.1)	2.7 (−0.3)
All TCs	36.0 (+1.4*)	959.1 (−3.5*)	18.9 (+1.0)

In each entry, the mean value for the simulated TCs in each cluster and all TCs are shown. The difference between simulation and observation (i.e., simulation minus observation) are represented in parenthesis. The asterisk (*) denotes the significant difference at the 99 % confidence level based on a Student's *t* test

that clusters C1 and C3 in Kim et al. (2011) seem to be merged into C1 in the present analysis because the genesis location and track shape of those in the previous study are the most similar among the other clusters.

The C1 includes the TCs generated in the northwestern Philippine Sea and re-curving at the East China Sea to affect East Asian countries such as eastern China, Taiwan, Korea, and Japan (Fig. 4a, b). It is worth noting that the track distribution was less fuzzy and re-curved more toward Japan in the simulation than in the observation. TCs generated in the southeastern Philippine Sea that re-curve over the ocean to the south of Japan and striking Korea and Japan were classified into C2 (Fig. 4c, d). The simulation showed less number of TC landfalls in Japan because the simulated track lengths are generally shorter than in observations. The TC detection criteria chosen to detect the realistic number of TCs may be too strict for detecting TCs in decaying stage, which may cause less landfall or shorter track lengths, which is a general limitation of TC detection method. This problem may be improved when the different criteria are used for TCs in different stages, which will be considered in future works. TCs in C3 were generated in the Philippine Sea and re-curved over the ocean to the east of Japan (Fig. 4e, f). C4 is characterized by track patterns similar to C3, but the genesis region and tracks were shifted farther eastward (Fig. 4g, h). The simulated TC-track distributions in these clusters are similar to that in the observation. TCs of straight-line tracks toward southeastern Asia (e.g. southern China, the Philippines, Vietnam, and Taiwan) were classified as C5 and C6 (Fig. 4i–l). These two clusters were separated on the basis of genesis locations and track lengths. The mean track reaches the coast of southern China in the observation, it reaches Taiwan in the simulation due to shorter tracks in C6. Overall, the simulated individual and mean tracks of the TC cluster agreed well with observations. Thus, it is meaningful to compare the observed and simulated characteristics, such as intensity and genesis frequency, of each TC cluster.

Table 1 presents the statistics of characteristics of the simulated and observed TC clusters. The maximum intensity, including the maximum surface wind speed and minimum central SLP, of the six TC clusters in the simulation agrees well with observations (at the 99 % confidence level) except for C2 and C5. C2 is the cluster of the strongest TCs in both observation (43.2 m s^{-1} and 940.3 hPa) and simulation (38.3 m s^{-1} and 952.0 hPa), but the simulation substantially underestimated the intensity of C2 compared with observations. Similarly, C5 in observation shows the weakest intensity (26.9 m s^{-1} and 980.6 hPa), but the simulation overestimates its intensity (34.6 m s^{-1} and 966.6 hPa). This explains the results discussed in Sect. 3.1; the frequency of extremely strong or weak TCs is underestimated (Fig. 2) because the intensities of C2 and C5 are not reasonable. The simulation also generated a similar number of TCs as in the observation for each cluster (at the 99 % confidence level) except for C1 and C2. The differences in the genesis frequency between simulation and observation were -1.0 and $+1.8$ for C1 and C2, respectively. Combining these two clusters, the errors in the TC genesis for C1 and C2 ($+0.8 = -1.0 + 1.8$) corresponded to 80 % of the total genesis error ($+1.0$).

These errors in simulating the spatial variations of TC activities indicate that the sum of C1 and C2 explains the major contribution. Here, C1 (C2) substantially underestimated (overestimated) the genesis and track frequency over the East China Sea (eastern Philippine Sea; Fig. 5a–d). The underestimated track frequency over the landfall zone of C2 (Fig. 5d) was due to the shorter tracks of C2 in the simulation. These errors in C1 and C2 are directly related to large variations in their genesis frequency (Table 1). In addition, these errors in C1 and C2 are similar to the underestimation (overestimation) over the East China Sea (southeastern Philippine Sea) in the total error (Fig. 3e, f). Thus, most of the regional discrepancy in TC activity appears to result from these two clusters. Interestingly, the overestimation of TC activity over the South China Sea (Fig. 3e, f)

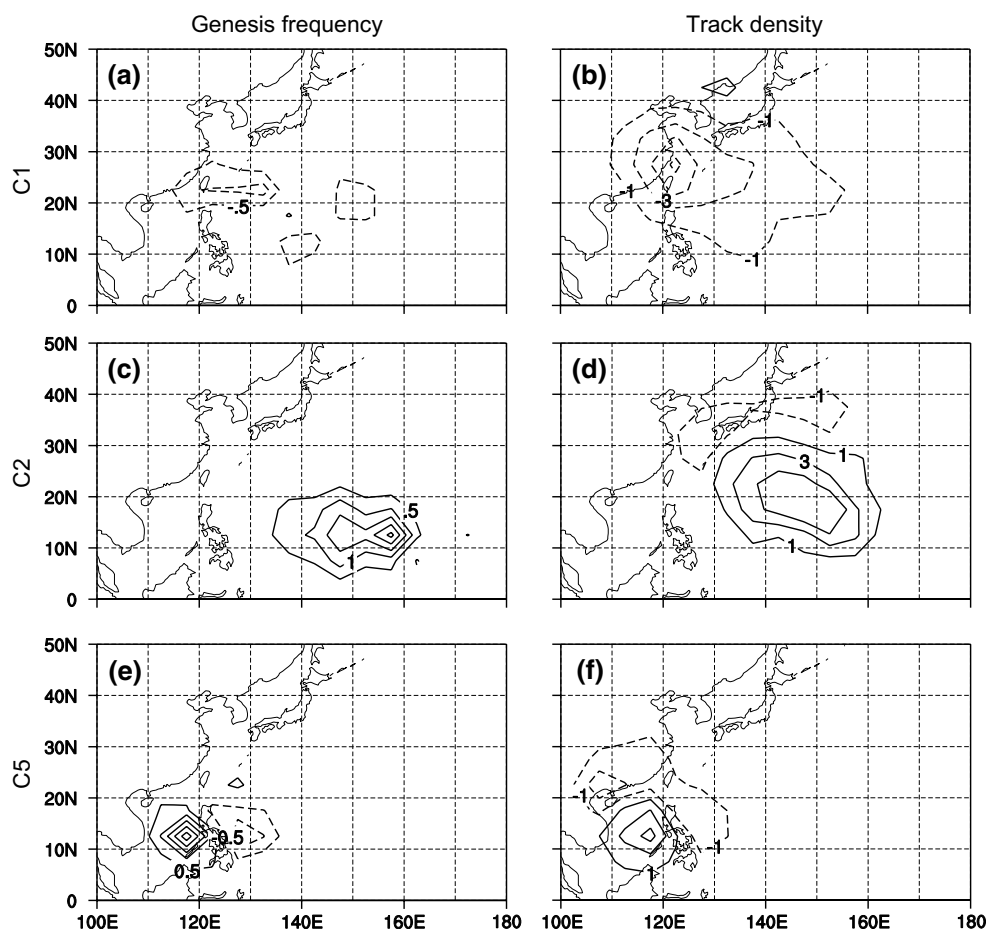


Fig. 5 Differences in TC genesis (*left*) and track (*right*) frequencies between simulation and observation as numbers per decade in a $5^\circ \times 5^\circ$ grid box for **a, b** C1, **c, d** C2, and **e, f** C5

is related to the bias in C5 (Fig. 5e, f) that shows only small difference in the genesis frequency (+0.3 per year or +9 for 29 years; Table 1). For C5, TC activities were overestimated over the South China Sea and underestimated over the western Philippine Sea, implying that the simulated genesis location of C5 is more toward the South China Sea compared with the observation. Model errors in genesis frequency (Table 1) and TC activity for the clusters other than C1 and C5 were insignificant (not shown).

3.3 Model errors in large-scale environments and the corresponding TCs

To investigate the causes for the errors in regional TC activities, large-scale environments that affect TC activities including zonal winds in the lower troposphere, wind strength in the upper troposphere, the location of the 5880-geopotential meter (gpm) height, vertical wind shear, and mid-level relative humidity were analyzed (Fig. 6). The simulated 850-hPa zonal wind pattern agreed well with the observation, but the westerlies over the tropical region were

too strong (Fig. 6a, b). These results imply the strengthening of the monsoon trough (Fig. 3e, f in JH13) and overestimation of wind convergence over the southeastern Philippine Sea. Most of the TCs can be generated in the southeastern Philippine Sea because the zonal wind convergence causes wave energy accumulation and enhances TC formation (Briegel and Frank 1997; Done et al. 2011). Thus, the overestimated TC genesis for C2 is definitely related to the overestimation of the strength of the monsoonal circulation. In addition, the western boundary of the subtropical North Pacific high, represented by the 5880-gpm line, was displaced to the east by more than 500 km compared with the observation (Fig. 6a, b) owing to the overestimated monsoon circulation. This weakening subtropical high also provided favorable large-scale environments for generating TCs with C2 track patterns.

Similarly, the 200-hPa wind speed pattern was reasonably simulated, except that the strength of mid-latitude jet stream was overestimated in the simulation (Fig. 6c, d). TCs can re-curve early in the mid-latitudes owing to the southward expansion of the subtropical jet which affects

Fig. 6 Climatological mean of **a, b** 850-hPa zonal wind with 5880-gpm line, **c, d** 200-hPa wind speed, **e, f** vertical wind shear, and **g, h** 600-hPa relative humidity for observation (*left*) and simulation (*right*)

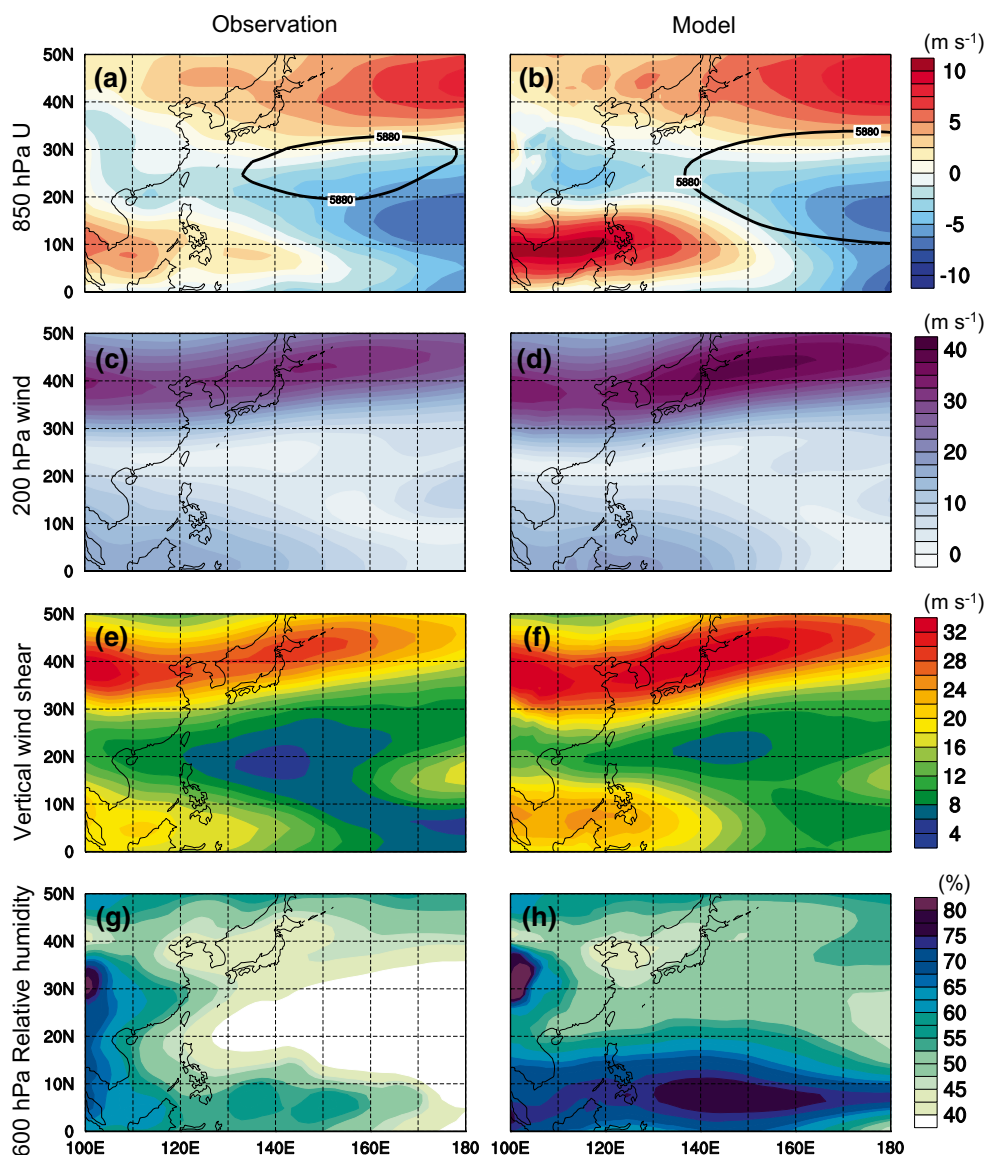


Table 2 The locations of re-curvature point of the mean tracks of C1, C2, and C3 in the observation and the simulation

	Observation		Simulation	
	Latitude (°N)	Longitude (°E)	Latitude (°N)	Longitude (°E)
C1	30.89	126.87	25.66	127.87
C2	25.46	138.67	24.73	141.26
C3	28.05	139.05	26.74	140.43

the point of TC re-curvature, causing the overestimation of C2. Conversely, these large-scale environments appeared to reduce the track frequency over the East Asian coastal region. The mean tracks of C1, C2, and C3 in the simulation showed earlier re-curvature than that in the observation (Table 2). C1 re-curved to the south, and C2 and C3 re-curved to the southeast compared with the observation.

Figure 6e, f illustrate the observed and simulated, respectively, vertical wind shear defined as the difference between the 850 and 200 hPa levels. Again, the simulation reasonably captured the general pattern of vertical wind shear but overestimated its magnitude over two regions: a subtropical region centered at 5°N and between 100°E and 140°E and a mid-latitude region extending from central China to northeastern Japan. Over the subtropical region, the simulated vertical wind shear is much stronger than the corresponding observations. This discrepancy may be induced by the strong westerly at the lower troposphere with enhanced monsoonal circulation in the simulation (Fig. 6b). Therefore, TC activity over that region can be controlled by the adverse effects of vertical wind shear (i.e., baroclinity), such as the ventilation and tilting-stabilization (DeMaria 1996), and the favorable effects of the monsoonal circulation. The positive effect of monsoonal circulation appears

to be dominant over the South China Sea, whereas the negative effect of vertical wind shear is dominant over the area east of the Philippine Sea, where TC activities are overestimated and underestimated in the simulation, respectively (Fig. 5e, f). The vertical wind shear in the simulation was slightly stronger than that in the observation to the east of 140°E; however, its magnitude was generally lower than 12 m s^{-1} , which is not a critical value as a constraint of TC genesis. Thus, the overestimation of TC genesis due to an enhanced monsoonal trough can be confined to the southeastern Philippine Sea region (east of 140°E), resulting in overestimation of the C2. At the mid-latitude region, the vertical wind shear over the East China Sea and south of the Korean Peninsula in the simulation was significantly stronger than that in the observation (Fig. 6f). This strong vertical wind shear zone related to the overestimated upper tropospheric winds (Fig. 6d) can reduce TC track pattern passing through that region, which can lead to decreased TC activity of the C1.

Lastly, the pattern of mid-level relative humidity was simulated reasonably (Fig. 6g, h), but the simulation excessively overestimated relative humidity over the tropical region (Fig. 6h). The local maximum of relative humidity appeared around 10°N and between 130°E and 160°E near the region where most of the C2s are generated. In addition, this high humidity condition continued vertically to the upper layer with enhanced upward motion at that region (not shown). Thus, the environment of high humidity and rising motions can cause the overestimation of C2 in the simulation. Conversely, the relative humidity at mid-latitude in the simulation was not similar to that in the observation. The simulated vertical motion was also weaker than that in the observation, particularly to the west of 130°E, which may be attributed to the southward expansion of the mid-latitude jet stream in the simulation (Fig. 6d). All of these large-scale environments indicate that the simulation tended to overestimate (underestimate) TC activities of the C2 (C1) type.

4 Conclusion

This study has examined the capability of the nested global–regional WRF model in studying TC activities over the WNP. The regional WRF model (50 km × 50 km horizontal resolution) nested within global WRF model simulations (150 km × 150 km) forced by initial and boundary conditions from the NCEP reanalysis-2 and OISST data has been run for the 29 TC seasons of 1982–2010. This study demonstrated that the model can produce realistic TCs with dynamical and thermal structures similar to those of observed TCs. The simulated TCs were clustered into six groups (C1 through C6) according to their track shapes

by using the fuzzy clustering to analyze the model's ability in detail. Evaluation of the simulated TC clusters against the clusters obtained from the observation suggests that the model generally produced reliable TC features except in few TC clusters. For TC intensity, the most noticeable model errors were noted in the simulation of extremely strong (C2) and weak (C5) TCs, mainly because of the coarse model resolution and the absence of ocean feedback in the simulation. We consider that these limitations can be resolved by using finer resolution and by coupling with an ocean model. General features of TC genesis and track were also simulated reasonably except for C1 and C2. These model errors are related to the large-scale environments that are extremely favorable for C2 but unfavorable for C1; these include enhanced monsoon trough, weakened subtropical high, southward expanded mid-latitude jet stream, high humidity over the tropical region, and strong vertical wind shear over mid-latitudes and tropical regions. The present results suggest the manner in which the model should be improved to accurately simulate TC activity. If the inherent errors of the large-scale environments examined in this study can be corrected, the model's performance would be improved significantly. However, it should be noted that these errors in C1 and C2 do not indicate that the model completely failed in the simulation. Rather, they suggest that the present stage of the model is imperfect. The overall model evaluation suggests that the global–regional WRF can be a useful tool for studying TC activities over the WNP, despite these shortcomings. Further studies on seasonal forecast of TC activities over the WNP can be conducted by using this model.

Acknowledgments This work was funded by the Korea Meteorological Administration Research and Development Program under Grant CATER 2012–2040.

References

- Au-Yeung AYM, Chan JCL (2011) Potential use of a regional climate model in seasonal tropical cyclone activity predictions in the western North Pacific. *Clim Dyn* 39:783–794
- Bender MA, Ginis I (2000) Real-case simulations of hurricane–ocean interaction using a high-resolution coupled model: effects on hurricane intensity. *Mon Weather Rev* 128:917–946
- Bender MA, Ginis I, Kurihara Y (1993) Numerical simulations of tropical cyclone–ocean interaction with a high-resolution coupled model. *J Geophys Res* 98:23245–23263
- Bengtsson L, Hodges KI, Esch M, Keenlyside N, Kornbluh L, Luo J-J, Yamagata T (2007) How many tropical cyclones change in a warmer climate? *Tellus A* 59:539–561
- Bensaid AM, Hall LO, Bezdek JC, Clarke LP, Silbiger ML, Arrington JA, Murtagh RF (1996) Validity-guided (re)clustering with applications to image segmentation. *IEEE Trans Fuzzy Syst* 4:112–123
- Bezdek JC (1981) Pattern recognition with fuzzy objective function algorithms. Kluwer Academic, Dordrecht 256

- Briegel LM, Frank WM (1997) Large-scale influences on tropical cyclogenesis in the western north Pacific. *Mon Weather Rev* 125:1397–1413
- Camargo SJ, Sobel AH (2005) Western North Pacific tropical cyclone intensity and ENSO. *J Clim* 18:2996–3006
- Camargo SJ, Li H, Sun L (2007a) Feasibility study for downscaling seasonal tropical cyclone activity using the NCEP regional spectral model. *Int J Clim* 27:311–325
- Camargo SJ, Robertson AW, Gaffney SJ, Smyth P, Ghil M (2007b) Cluster analysis of typhoon tracks. Part I: General properties. *J Clim* 20:3635–3653
- Camargo SJ, Robertson AW, Gaffney SJ, Smyth P, Ghil M (2007c) Cluster analysis of typhoon tracks. Part II: large-scale circulation and ENSO. *J Clim* 20:3654–3676
- Cha D-H, Jin C-S, Lee D-K, Kuo Y-H (2011) Impact of intermittent spectral nudging on regional climate simulation using Weather Research and Forecasting model. *J Geophys Res* 116. doi:10.1029/2010jd015069
- Chan JCL (2000) Tropical cyclone activity over the western North Pacific associated with El Niño and La Niña events. *J Clim* 13:2960–2972
- Chen F, Dudhia J (2001) Coupling an advanced land surface-hydrology model with the Penn State-NCAR MM5 modeling system. Part I: model implementation and sensitivity. *Mon Weather Rev* 129:569–585
- Collins WD, Rasch PJ, Boville BA, Hack JJ, McCaa JR, Williamson DL, Kiehl JT, Briegleb B, Bitz C, Lin S-J, Zhang M, Dai Y (2004) Description of the NCAR Community Atmosphere Model (CAM 3.0). NCAR Tech. Note. NCAR Tech. Note 226
- Davis C, Wang W, Chen SS, Chen Y, Corbosiero K, DeMaria M, Dudhia J, Holland G, Klemp J, Michalakes J, Reeves H, Rotunno R, Snyder C, Xiao Q (2008) Prediction of landfalling hurricanes with the advanced hurricane WRF model. *Mon Weather Rev* 136:1990–2005
- DeMaria M (1996) The effect of vertical shear on tropical cyclone intensity change. *J Atmos Sci* 53:2076–2087
- Done JM, Holland GJ, Webster PJ (2011) The role of wave energy accumulation in tropical cyclogenesis over the tropical North Atlantic. *Clim Dyn* 36:753–767
- Dunn JC (1973) A fuzzy relative of the ISODATA process and its use in detecting compact well-separated clusters. *J Cybernet* 3:32–57
- Elsner JB, Liu KB (2003) Examining the ENSO-typhoon hypothesis. *Clim Res* 25:43–54
- Fierro AO, Rogers RF, Marks FD, Nolan DS (2009) The impact of horizontal grid spacing on the microphysical and kinematic structures of strong tropical cyclones simulated with the WRF-ARW model. *Mon Weather Rev* 137:3717–3743
- Frank WM (1977) Structure and energetics of tropical cyclone I. Storm structure. *Mon Weather Rev* 105:1119–1135
- Gentry MS, Lackmann GM (2010) Sensitivity of simulated tropical cyclone structure and intensity to horizontal resolution. *Mon Weather Rev* 138:688–704
- Gray WM (1977) Tropical cyclone genesis in the western North Pacific. *Meteorol Atmos Phys* 55:465–482
- Harr PA, Elsberry RL (1991) Tropical cyclone track characteristics as a function of large-scale circulation anomalies. *Mon Weather Rev* 119:1448–1468
- Ho CH, Baik JJ, Kim JH, Gong DY, Sui CH (2004) Interdecadal changes in summertime typhoon tracks. *J Clim* 17:1767–1776
- Ho C-H, Kim H-S, Jeong J-H, Son S-W (2009) Influence of stratospheric quasi-biennial oscillation on tropical cyclone tracks in the western North Pacific. *Geophys Res Lett* 36. doi:10.1029/2009gl0137163
- Hodanay S, Gray WM (1993) An observational analysis of tropical cyclone recurvature. *Mon Weather Rev* 121:2665–2689
- Hong SY, Dudhia J, Chen SH (2004) A revised approach to ice microphysical processes for the bulk parameterization of clouds and precipitation. *Mon Weather Rev* 132:103–120
- Hong SY, Noh Y, Dudhia J (2006) A new vertical diffusion package with an explicit treatment of entrainment processes. *Mon Weather Rev* 134:2318–2341
- Jin C-S, Ho C-H, Kim J-H, Lee D-K, Cha D-H, Yeh S-W (2013) Critical role of northern off-equatorial sea surface temperature forcing associated with central Pacific El Niño in more frequent tropical cyclone movements toward east Asia. *J Clim* 26:2534–2545
- Kain JS, Fritsch JM (1990) A one-dimensional entraining detraining plume model and its application in convective parameterization. *J Atmos Sci* 47:2784–2802
- Kanamitsu M, Ebisuzaki W, Woollen J, Yang S-K, Hnilo JJ, Fiorino M, Potter GL (2002) NCEP–DOE AMIP-II reanalysis (R-2). *Bull Am Meteorol Soc* 83:1631–1643
- Keptert JD (2006a) Observed boundary layer wind structure and balance in the hurricane core. Part I: Hurricane Georges. *J Atmos Sci* 63:2169–2193
- Keptert JD (2006b) Observed boundary layer wind structure and balance in the hurricane core. Part II: hurricane Mitch. *J Atmos Sci* 63:2194–2211
- Kim JH, Ho CH, Sui CH (2005a) Circulation features associated with the record-breaking typhoon landfall on Japan in 2004. *Geophys Res Lett* 32. doi:10.1029/2005gl022494
- Kim JH, Ho CH, Sui CH, Park SK (2005b) Dipole structure of inter-annual variations in summertime tropical cyclone activity over East Asia. *J Clim* 18:5344–5356
- Kim J-H, Ho C-H, Kim H-S, Sui C-H, Park SK (2008) Systematic variation of summertime tropical cyclone activity in the western North Pacific in relation to the Madden–Julian Oscillation. *J Clim* 21:1171–1191
- Kim H-S, Kim J-H, Ho C-H, Chu P-S (2011) Pattern classification of typhoon tracks using the fuzzy c-means clustering method. *J Clim* 24:488–508
- Kim J, Waliser DE, Mattmann CA, Goodale CE, Hart AF, Zimdars PA, Crichton DJ, Jones C, Nikulin G, Hewitson B, Jack C, Leonard C, Favre A (2013) Evaluation of the CORDEX-Africa multi-RCM hindcast: systematic model errors. *Clim Dyn*. doi:10.1007/s00382-013-1751-7
- Manganello JV, Hodges KI, Kinter JL, Cash BA, Marx L, Jung T, Achuthavarier D, Adams JM, Altschuler EL, Huang B, Jin EK, Stan C, Towers P, Wedi N (2012) Tropical cyclone climatology in a 10-km global atmospheric GCM: toward weather-resolving climate modeling. *J Clim* 25:3867–3893
- Mearns LO, Arritt R, Biner S, Bukovsky MS, McGinnis S, Sain S, Caya D, Correia J, Flory D, Gutowski W, Takle ES, Jones R, Leung R, Moufouma-Okia W, McDaniel L, Nunes AMB, Qian Y, Roads J, Sloan L, Snyder M (2012) The north American regional climate change assessment program overview of phase I results. *Bull Am Meteorol Soc* 93:1337–1362
- Nakamura J, Lall U, Kushnir Y, Camargo SJ (2009) Classifying north Atlantic tropical cyclone tracks by mass moments. *J Clim* 22:5481–5494
- Oouchi K, Yoshimura J, Yoshimura H, Mizuta R, Kusunoki S, Noda A (2006) Tropical cyclone climatology in a global-warming climate as simulated in a 20 km-mesh global atmospheric model: frequency and wind intensity analyses. *J Meteorol Soc Jpn* 84:259–276
- Park DSR, Ho CH, Kim JH (2014) Growing threat of intense tropical cyclones to East Asia over the period 1977–2010. *Environ Res Lett* 9:ArtN 014008. doi:10.1088/1748-9326/9/1/014008
- Potty J, Oo SM, Raju PVS, Mohanty UC (2012) Performance of nested WRF model in typhoon simulations over West Pacific and South China Sea. *Nat Hazards* 63:1451–1470

- Ray P, Zhang CD, Moncrieff MW, Dudhia J, Caron JM, Leung LR, Bruyere C (2011) Role of the atmospheric mean state on the initiation of the Madden–Julian Oscillation in a tropical channel model. *Clim Dyn* 36:161–184
- Reynolds RW, Rayner NA, Smith TM, Stokes DC, Wang WQ (2002) An improved in situ and satellite SST analysis for climate. *J Clim* 15:1609–1625
- Shin HH, Hong SY, Dudhia J, Kim YJ (2010) Orography-induced gravity wave drag parameterization in the global WRF: implementation and sensitivity to shortwave radiation schemes. *Adv Meteorol Artn* 959014. doi:[10.1155/2010/959014](https://doi.org/10.1155/2010/959014)
- Skamarock WC, Kelpm JB, Gill DO, Barker DM, Duda MG, Huang XY, Wang W, Powers JG (2008) A description of the advanced research wrf version 3. NCAR Tech. Note NCAR/TN-475+STR:133
- Skok G, Tribbia J, Rakovec J (2010) Object-based analysis and verification of WRF model precipitation in the low- and midlatitude Pacific Ocean. *Mon Weather Rev* 138:4561–4575
- Stowasser M, Wang Y, Hamilton K (2007) Tropical cyclone changes in the western North Pacific in a global warming scenario. *J Clim* 20:2378–2396
- Suzuki-Parker A (2011) An assessment of uncertainties and limitations in simulating tropical cyclone climatology and future changes. Ph.D. thesis Georgia Institute of Technology 78
- Tulich SN, Kiladis GN, Suzuki-Parker A (2011) Convectively coupled Kelvin and easterly waves in a regional climate simulation of the tropics. *Clim Dyn* 36:185–203
- Waliser D, Kim J, Xue Y, Chao Y, Eldering A, Fovell R, Hall A, Li Q, Liou KN, McWilliams J, Kapnick S, Vasic R, Sale F, Yu Y (2011) Simulating cold season snowpack: impacts of snow albedo and multi-layer snow physics. *Clim Change* 109:95–117
- Walsh K, Lavender S, Murakami H, Scoccimarro E, Caron L-P, Ghan-tous M (2010) The tropical cyclone climate model intercomparison project. *Hurricanes Clim Change* 1–24
- Wang B, Chan JCL (2002) How strong ENSO events affect tropical storm activity over the western North Pacific. *J Clim* 15:1643–1658
- Wang Y, Wu CC (2004) Current understanding of tropical cyclone structure and intensity changes—a review. *Meteorol Atmos Phys* 87:257–278
- Xie XLL, Beni G (1991) A validity measure for fuzzy clustering. *Trans Pattern Anal Mach Intell* 13:841–847